RSC Advances

ROYAL SOCIETY OF CHEMISTRY

www.rsc.org/advances

Ferroelastic property of tetramethylammonium tetrachlorozincate tetrachlorocuprate, $[N(CH_3)_4]_2Zn_{1-x}Cu_xCl_4$ (x = 0, 0.1, 0.3, 0.5, and 1)

Ae Ran Lim[1,2,*]

[1]*Department of Science Education, Jeonju University, Jeonju 560-759, Korea*

[2]*Department of Carbon Fusion Engineering, Jeonju University, Jeonju 560-759, Korea*

---

[*]To whom all correspondence should be addressed

Tel : +82-(0)63-220-2514

Fax: +82-(0)63-220-2053

E-mail: aeranlim@hanmail.net

arlim@jj.ac.kr

Keywords: $[N(CH_3)_4]_2ZnCl_4$, $[N(CH_3)_4]_2CuCl_4$, Ferroelastic, Nuclear magnetic resonance, CP/MAS NMR, Phase transition, Crystal growth,

ABSTRACT

The various crystallographic structures of $[N(CH_3)_4]_2Zn_{1-x}Cu_xCl_4$ (x=0, 0.1, 0.3, 0.5, and 1) may be understood by considering the different chemical shifts observed in ^1H MAS and ^{13}C CP/MAS NMR spectra. Cu^{2+} ions, after replacing partially the Zn^{2+} ions, occupy the same locations in the lattice as the Zn^{2+} ions. The NMR spectrum and $T_{1\rho}$ of x=0.1 and 0.3 were found to be similar to those of pure $[N(CH_3)_4]_2ZnCl_4$, whereas the NMR spectrum and $T_{1\rho}$ of x=0.5 were different. Consequently, the existence of ferroelastic properties of $N(CH_3)_4$ ions in x=0, 0.1, 0.3, and 1 are apparent at low temperatures, whereas they disappear for x=0.5. It has been demonstrated that the replacement of Zn^{2+} ions with high concentrations of Cu^{2+} ions changes the ferroelastic property of the crystal.

I. INTRODUCTION

Crystals of the formula A_2BX_4 have received a great deal of attention owing to their interesting phase transition sequences. $[N(CH_3)_4]_2ZnCl_4$ and $[N(CH_3)_4]_2CuCl_4$ single crystals are A_2BX_4-type crystals. Tetramethylammonium tetrachlorozincate, $[N(CH_3)_4]_2ZnCl_4$, undergoes five phase transitions at the following temperatures: 161 K (T_{C5}), 181 K (T_{C4}), 276.3 K (T_{C3}), 279 K (T_{C2}), and 296 K (T_{C1}).[1-7] These previous studies have concluded that there are six phases, I to VI in the order of decreasing temperature, of $[N(CH_3)_4]_2ZnCl_4$ crystals. The crystal structure of phase I is orthorhombic. The transition from the normal (I) to the incommensurate (II) phase occurs at 296 K. The corresponding symmetry changes are as follows: the ferroelectric phase III is orthorhombic with space group $P2_1cn$; the ferroelastic phase IV is monoclinic with space group $P2_1/n$; the ferroelastic phase V is monoclinic with space group $P2_1/c$; and finally, phase VI is orthorhombic with space group $P2_12_12_1$.[5] Furthermore, tetramethylammonium tetrachlorocuprate, $[N(CH_3)_4]_2CuCl_4$, crystals exhibit four phases, I to IV, with transition temperatures of 263 K (T_{C3}), 291 K (T_{C2}), and 301 K (T_{C1}).[8] The structure and space group of the lowest temperature phase IV is monoclinic with space group $P112_1/n$. The structure of phase III is monoclinic with space group $P12_1/c1$, and phase II is incommensurate. The highest temperature phase, phase I, has an orthorhombic structure with space group $Pmcn$. These three phase transitions in $[N(CH_3)_4]_2CuCl_4$ are, in the order of increasing temperature: ferroelastic (IV)–ferroelastic (III), ferroelastic (III)–incommensurate (II), and incommensurate (II)–commensurate (I).[9] In particular, these two compounds, $[N(CH_3)_4]_2ZnCl_4$ and $[N(CH_3)_4]_2CuCl_4$, have the ferroelastic property at low temperatures.

Ferroelasticity was first recognized as a structure property by Aizu in 1970.[10] A crystal is ferroelastic if it has two or more stable orientation states in the absence of mechanical stress, and can be reversibly transformed from one to another of these states by the application of mechanical stress. When a ferroelastic crystal is heated, the ferroelastic effect usually disappears at a well-defined temperature. At this temperature, a structural phase transition occurs between a ferroelastic and a paraelastic phase; the main feature of which is that a ferroelastic hysteresis exists in one phase but not in the other. Also, the ferroelastic domain occurs in all ferroelastic crystals as a consequence of the reduction in symmetry between the paraelastic and ferroelastic phases.

The physical properties of $[N(CH_3)_4]_2ZnCl_4$ and $[N(CH_3)_4]_2CuCl_4$ have been studied using various experimental methods by several research groups.[11-20] Ribet et al. [21] reported observing ferroelectric-ferroelastic phase transitions of $[N(CH_3)_4]_2ZnCl_4$ through X-ray and synchrotron topography. Recently, the roles of chemically inequivalent a-$N(CH_3)_4$ and b-$N(CH_3)_4$ ions in $[N(CH_3)_4]_2ZnCl_4$ and $[N(CH_3)_4]_2CuCl_4$ have been reported by static nuclear magnetic resonance (NMR) and magic angle spinning (MAS) NMR, respectively.[22, 23] Furthermore, the ferroelastic phase transition of $[N(CH_3)_4]_2ZnCl_4$ and $[N(CH_3)_4]_2CuCl_4$ at low temperatures have been discussed.[24]

In this work, $[N(CH_3)_4]_2Zn_{1-x}Cu_xCl_4$ (x=0, 0.1, 0.3, 0.5, and 1) single crystals were grown from aqueous solutions by the slow evaporation method. We measured the temperature dependences for ^1H magic angle spinning (MAS) NMR spectrum and ^{13}C cross-polarization (CP)/MAS NMR spectrum of $[N(CH_3)_4]_2Zn_{1-x}Cu_xCl_4$ to elucidate the structural geometry. In addition, we determined the spin-lattice relaxation times in the rotating frame, $T_{1\rho}$, for ^1H and ^{13}C nuclei in $[N(CH_3)_4]_2Zn_{1-x}Cu_xCl_4$, for varying amounts of impurity Cu^{2+} ions. This is the first time that the local structures of $[N(CH_3)_4]_2Zn_{1-x}Cu_xCl_4$ have been investigated, and we used the results to analyze the role of $N(CH_3)_4$ ions. These results enabled us to compare the structural properties of pure $[N(CH_3)_4]_2ZnCl_4$ and $[N(CH_3)_4]_2CuCl_4$, and examine the effect of substituting Zn^{2+} ions in $[N(CH_3)_4]_2ZnCl_4$ with Cu^{2+} ions, with a focus on the effects of such substitution on ferroelasticity. Furthermore, in order to confirm the ferroelastic properties, domain structures were observed using an optical polarizing microscope.

II. CRYSTAL STRUCTURE

At room temperature, the $[N(CH_3)_4]_2Zn_{0.5}Cu_{0.5}Cl_4$ crystal is an orthorhombic system (space group $P2_1cn$) with Z=4 and the following unit cell dimensions: a= 8.988 Å, b=15.527 Å, and c=12.269 Å.[25] The atomic arrangement in $[N(CH_3)_4]_2Zn_{0.5}Cu_{0.5}Cl_4$ consists of alternate organic-inorganic layers of a-$N(CH_3)_4$/ $Zn(Cu)Cl_4$ and organic sheets b-$N(CH_3)_4$, both parallel to b-plane (Fig. 1).[26] This figure shows chains that are repeated sequences of $Cu(Zn)Cl_4$ and a-$N(CH_3)_4$, where the sense of tetrahedron orientation alternates within the same chain. The b-$N(CH_3)_4$ tetrahedra are present between the chains and on both sides of the organic-inorganic layers, building organic layers.

A $[N(CH_3)_4]_2ZnCl_4$ crystal in phase I has an orthorhombic structure with space group *Pmcn*. Its orthorhombic lattice constants are: a=8.946 Å, b=15.515 Å, and c= 12.268 Å.[27, 28] In this phase, a unit cell contains Z=4 units consisting of two inequivalent kinds of tetramethylammonium ions, hereafter abbreviated as a-$N(CH_3)_4$ and b-$N(CH_3)_4$, and one kind of $ZnCl_4^{2-}$ ion.[27] The $ZnCl_4$ ion and the a-$N(CH_3)_4$ are positioned in a strongly correlated manner, while the b-$N(CH_3)_4$ is less correlated than the other kind of ions. Moreover, a $[N(CH_3)_4]_2CuCl_4$ crystal in phase I has an orthorhombic structure, and its orthorhombic lattice constants are: a=9.039 Å, b= 15.515 Å, and c=12.268 Å, which are slightly different from those for the hexagonal form.[29, 30] In this phase, a unit cell contains Z=4 units consisting of two inequivalent kinds of tetramethylammonium ions, as well as $[N(CH_3)_4]_2ZnCl_4$.

III. EXPERIMENTAL METHOD

$[N(CH_3)_4]_2Zn_{1-x}Cu_xCl_4$ (x=0, 0.1, 0.3, 0.5, and 1) single crystals were grown at room temperature by slow evaporation of an aqueous solution containing $ZnCl_2$, $CuCl_2$, and $N(CH_3)_4Cl$, in stoichiometric proportions. $[N(CH_3)_4]_2Zn_{1-x}Cu_xCl_4$ single crystals varied in color according to the amount of Cu^{2+} ions, as shown in Fig. 2.

Solid-state NMR experiments were performed using a Bruker DSX 400 FT NMR spectrometer at the Korea Basic Science Institute. ^1H MAS NMR and ^{13}C CP/MAS NMR experiments were performed at the Larmor frequencies of 400.12 MHz and 100.61 MHz, respectively. The samples were placed in the 4 mm CP/MAS probe as powders. The MAS rate was set to 10 kHz and 7 kHz for ^1H MAS and ^{13}C CP/MAS, respectively, to minimize the spinning sideband overlap. Here, the frequency scale of the spectrum for ^1H and ^{13}C was expressed with respect to tetramethylsilane (TMS). In the case for ^1H, the $T_{1\rho}$ measurements were performed using $\pi/2-t-$acqusition. The spin–lattice relaxation times in the rotating frame, $T_{1\rho}$, were measured by varying the length of the spin-locking pulses. The $\pi/2$ pulse width used for $T_{1\rho}$ was 5 μs, corresponding to the frequency of the spin-locking field, 50 kHz. Moreover, the $T_{1\rho}$ for ^{13}C was obtained using CP–t–acquisition, and the frequency of the spin-locking field was 78.1 kHz. The experimental temperatures were maintained at constant values, with an accuracy of ±0.5 K, by controlling the nitrogen gas flow and heater current. The temperature-dependent NMR measurements were carried out in the temperature range from 150 to 450 K.

IV. EXPERIMENTAL RESULTS AND ANALYSIS

At room temperature, the structures of the $[N(CH_3)_4]_2Zn_{1-x}Cu_xCl_4$ (x=0, 0.1, 0.3, 0.5, and 1) crystals were determined with an X-ray diffraction system (Bruker AXS GMBH) at the Korea Basic Science Institute. The single crystals were mounted on a Bruker SMART CCD diffractometer equipped with a graphite-monochromated Mo Kα (λ = 0.71073 Å) radiation source. Data collection and integration were performed at 298 K with SMART (Bruker, 2000) and SAINT-Plus (Bruker, 2001).[31] The lattice constants of the five crystals were shown in Table 1, and all the $[N(CH_3)_4]_2Zn_{1-x}Cu_xCl_4$ crystals containing Cu^{2+} impurities had the same orthorhombic structure as $[N(CH_3)_4]_2ZnCl_4$ and $[N(CH_3)_4]_2CuCl_4$. And, the chemical composition of the crystals was confirmed with an electron probe microanalyzer (EPMA 1600). The X-ray diffraction and elemental analysis data indicate that these single crystals are $[N(CH_3)_4]_2Zn_{1-x}Cu_xCl_4$ (x=0.1, 0.3, and 0.5). In addition, in order to determine the phase transition temperatures, differential scanning calorimetry (DSC) was carried out on the crystals with a Dupont 2010 DSC instrument. The measurements were performed at a heating rate of 10 ºC/min in the temperature range from 200 K to 500 K, and the endothermic peaks for x=0.1, 0.3, and 0.5 were shown in Fig. 3. The phase transition temperatures are nearly unchanged with varying amounts of impurity Cu^{2+} ions and are similar to those for pure $[N(CH_3)_4]_2ZnCl_4$.

A. ^{1}H MAS NMR in $[N(CH_3)_4]_2Zn_{1-x}Cu_xCl_4$ (x = 0, 0.1, 0.3, 0.5, and 1)

Structural analysis of $[N(CH_3)_4]_2Zn_{1-x}Cu_xCl_4$ (x=0, 0.1, 0.3, 0.5, and 1) was carried out with the ^{1}H MAS NMR method. The chemical shifts for ^{1}H in $[N(CH_3)_4]_2Zn_{1-x}Cu_xCl_4$ (x=0, 0.1, 0.3, and 0.5) were measured over the temperature range of 180–425 K, as shown in Fig. 4(a). In the cases of x=0, 0.1, 0.3, and 0.5, the small changes in the chemical shifts near 296 K correspond to phase transitions. The chemical shift of $[N(CH_3)_4]_2Zn_{0.9}Cu_{0.1}Cl_4$ with x=0.1 changes near 276 K, meaning structural phase transition. However, the other phase transitions cannot be identified from the chemical shifts. Alternatively, the insert in Fig. 4(b) shows the ^{1}H MAS NMR spectrum of $[N(CH_3)_4]_2CuCl_4$ with x=1 at room temperature. The NMR spectrum consists of two peaks at chemical shifts of 2.45 and 6.80 ppm. The spinning sidebands are marked with asterisks. The signals at chemical shifts of 2.45 and 6.80 ppm are assigned to the methyl protons, and they are clearly due to magnetically

inequivalent sites. Here, the two proton peaks at 2.45 and 6.80 ppm cannot be distinguished between a-$N(CH_3)_4$ or b-$N(CH_3)_4$. The ^1H chemical shift changes with increasing temperature, as shown in Fig. 4(b). The chemical shifts near T_{C3} also change abruptly, whereas those near T_{C1} and T_{C2} change almost continuously. The chemical shift in the case for x=1 is completely different from those for x=0, 0.1, 0.3, and 0.5. This difference is due to variations in the electronic structure of the Zn^{2+} and Cu^{2+} ions.

The spin-lattice relaxation times in the rotating frame, $T_{1\rho}$, for the proton in $[N(CH_3)_4]_2Zn_{1-x}Cu_xCl_4$ (x=0, 0.3, 0.5, and 1) were obtained as a function of temperature. The nuclear magnetization recovery curves obtained for protons were described by the following single exponential function:[32-34] $S(t)=S_0\exp(-t/T_{1\rho})$, where S(t) is the magnetization at time, t, and S_0 is the total nuclear magnetization of ^1H at thermal equilibrium. The slopes of the recovery traces are different at each temperature. The temperature dependences of the ^1H $T_{1\rho}$ are shown in Fig. 5. When the paramagnetic Cu^{2+} impurity was included, x=0.3 in $[N(CH_3)_4]_2Zn_{1-x}Cu_xCl_4$, the trend in $T_{1\rho}$ resembles that of ^1H $T_{1\rho}$ in pure $[N(CH_3)_4]_2ZnCl_4$. Below T_{C3}, $T_{1\rho}$ increases abruptly, and the proton $T_{1\rho}$ data does not show any evidence of an anomalous change near the phase transition temperatures of T_{C1} and T_{C2}. However, the ^1H $T_{1\rho}$ curve of $[N(CH_3)_4]_2Zn_{0.5}Cu_{0.5}Cl_4$ is markedly different from those observed for pure $[N(CH_3)_4]_2ZnCl_4$ and $[N(CH_3)_4]_2CuCl_4$. Here, the ^1H $T_{1\rho}$ values for $[N(CH_3)_4]_2Zn_{0.5}Cu_{0.5}Cl_4$ are smaller than those in $[N(CH_3)_4]_2ZnCl_4$, and larger than that in $[N(CH_3)_4]_2CuCl_4$. In the case for $[N(CH_3)_4]_2CuCl_4$ with x=1, the ^1H $T_{1\rho}$ was found to be much shorter than that for $[N(CH_3)_4]_2ZnCl_4$. The $T_{1\rho}$ values increase with increasing temperature and the change is discontinuous near T_{C3}, but relatively continuous near T_{C1} and T_{C2}.

B. ^{13}C CP/MAS NMR in $[N(CH_3)_4]_2Zn_{1-x}Cu_xCl_4$ (x = 0, 0.1, 0.3, 0.5, and 1)

Structural analysis of $[N(CH_3)_4]_2Zn_{1-x}Cu_xCl_4$ (x=0, 0.1, 0.3, 0.5, and 1) was carried out using ^{13}C NMR spectroscopy. The chemical shifts for ^{13}C in $[N(CH_3)_4]_2Zn_{1-x}Cu_xCl_4$ (x=0, 0.1, 0.3, and 0.5) were measured over the temperature range of 170–430 K, as shown in Fig. 6(a). In the cases for x=0, 0.1, 0.3, and 0.5, the ^{13}C CP/MAS NMR spectrum in the temperature range 293–380 K consists of a single resonance line for one type of $N(CH_3)_4$, as shown in Fig. 6(a). The chemical shifts of CH_3 in the two inequivalent kinds of a-$N(CH_3)_4$ and b-$N(CH_3)_4$ in $[N(CH_3)_4]_2Zn_{1-x}$

Cu_xCl_4 (x=0, 0.1, 0.3, and 0.5) were not measured within this temperature range. In the case for $[N(CH_3)_4]_2Zn_{1-x}Cu_xCl_4$ (x=0, 0.1, and 0.3), the ^{13}C NMR chemical shift at the transition point of 276 K (=T_{C3}) splits into two lines, as shown in Fig. 6(a). This splitting indicates that at this temperature there is a phase transition to a new phase with a monoclinic symmetry lower than the orthorhombic symmetry. The III-IV transition results in an abrupt splitting of the ^{13}C NMR line into two components, indicative of a ferroelastic property. The ferroelastic domain structures in phase IV of $[N(CH_3)_4]_2ZnCl_4$ (x=0) and $[N(CH_3)_4]_2Zn_{0.7}Cu_{0.3}Cl_4$ (x=0.3) were confirmed by employing an optical polarizing microscope. Figure 6(c) shows the domain patterns for the ferroelastic and paraelastic phases of x=0 and x=0.3. The domain patterns at 350 K do not appear similar to those for the paraelectric phase. The appearance of microscope domain walls with many parallel lines with decreasing temperature is a property of the ferroelastic phase. In the case for $[N(CH_3)_4]_2Zn_{0.5}Cu_{0.5}Cl_4$ (x=0.5), the ^{13}C NMR spectrum at all temperatures measured here consists of only one resonance line, as shown in Fig. 6(a). The in-situ ^{13}C CP/MAS NMR spectrum for $[N(CH_3)_4]_2Zn_{0.5}Cu_{0.5}Cl_4$ are also shown in Fig. 6(b) as a function of temperature. Furthermore, there were only continuous quantitative changes in the chemical shift, where the ^{13}C chemical shift slowly and monotonically increases with temperature. In the case for $[N(CH_3)_4]_2Zn_{0.5}Cu_{0.5}Cl_4$ with x=0.5 the domain walls did not appear at all temperatures, as shown in Fig. 6(c).

On the other hand, the ^{13}C CP/MAS NMR spectrum for $[N(CH_3)_4]_2CuCl_4$ at room temperature has two signals at chemical shifts of δ = 72.13 and 133.48 ppm. The signals at chemical shifts of δ=72.13 and 133.48 ppm represent the methyl carbons in inequivalent b-$N(CH_3)_4$ and a-$N(CH_3)_4$, respectively. In the X-ray diffraction study of Hasebe et al.[10], the deformation of the b-$N(CH_3)_4$ ion was larger than that for the a-$N(CH_3)_4$ ion, and the degree of the deformation was enlarged in the ferroelectric phase. Based on these results, a-$N(CH_3)_4$ and b-$N(CH_3)_4$ are defined according the change of the relaxation time as a function of temperature, which is discussed next. Figure 7(a) shows the ^{13}C CP/MAS NMR spectrum below 291 K, in which the ^{13}C chemical shifts are shown by the three lines. Above T_{C2} (291 K), the ^{13}C NMR spectrum consists of two lines for a-$N(CH_3)_4$ and b-$N(CH_3)_4$, as shown in Fig. 7(a). However, at the transition point at 291 K, the ^{13}C NMR chemical shifts split into three lines. This splitting indicates that there is a phase transition at this temperature to a new phase with monoclinic symmetry, which is a symmetry reduction from orthorhombic

symmetry. Thus, the II-III transition results in an abrupt splitting of the ^{13}C NMR line into three components, which is indicative of ferroelasticity. Furthermore, above 291 K, there were only continuous quantitative changes in the chemical shift, where the ^{13}C chemical shift slowly and monotonically decreases with increasing temperature. The ferroelastic domain structures in phases III and IV of $[N(CH_3)_4]_2CuCl_4$ with x=1 were observed by employing an optical polarizing microscope, as shown in Fig. 7(b). The domain walls in the ferroelastic phase of phase IV were measured, whereas those in the paraelastic phase of phase I had disappeared. Consequently, the NMR spectrum and domain walls of $[N(CH_3)_4]_2Zn_{1-x}Cu_xCl_4$ (x=0, 0.1, 0.3, and 1) below 276 K show the ferroelastic characteristic, whereas the NMR spectrum and domain patterns of $[N(CH_3)_4]_2Zn_{0.5}Cu_{0.5}Cl_4$ below 276 K do not.

The spin-lattice relaxation times in the rotating frame, $T_{1\rho}$, in the $[N(CH_3)_4]_2Zn_{1-x}Cu_xCl_4$ (x=0, 0.3, 0.5, and 1) were obtained for each carbon as a function of temperature, with variable spin locks on the carbon channel following cross-polarization. The ^{13}C magnetization was generated by cross-polarization, after spin locking of the protons. The proton field was then turned off for a variable time, t, while the ^{13}C rf field remained on. Finally, the ^{13}C free induction decay was observed under high-power proton decoupling, and a Fourier transform was subsequently applied. Values of $T_{1\rho}$ could be selected by the Fourier transformation of the free-induction decay (FID), after spin locking and repetition of the experiment with variations in the time, t. The signals obtained for carbon were described by a single exponential function. Figure 8(a) shows the $T_{1\rho}$ values for ^{13}C in the cases of x=0, 0.3, and 0.5. The slopes of the $T_{1\rho}$ values near 296 K (=T_{C1}) are different, and this temperature corresponds to phase transition. The $T_{1\rho}$ values for two ^{13}C signals in the ferroelastic phase are nearly the same within the experimental error range. In the case for $[N(CH_3)_4]_2CuCl_4$ with x=1, the ^{13}C $T_{1\rho}$ values for a-$N(CH_3)_4$ and b-$N(CH_3)_4$, shown in Fig. 8(b), are similar, especially at higher temperatures. However, near T_{C3}, the $T_{1\rho}$ values change abruptly, and the $T_{1\rho}$ values for the two ^{13}C signals of b-$N(CH_3)_4$, produced by the ferroelastic twin structure below T_{C2}, are the same within the experimental error range.

V. DISCUSSION

The structures and the phase transition temperatures of the mixed crystals $[N(CH_3)_4]_2Zn_{1-x}Cu_xCl_4$ (x=0, 0.1, 0.3, 0.5, and 1) were determined with X-ray diffraction and DSC, respectively. Here, the structure or phase transition temperatures were almost unchanged by the doping of $[N(CH_3)_4]_2ZnCl_4$ crystals with Cu^{2+} ions.

The chemical shifts for ^1H and ^{13}C nuclei in $[N(CH_3)_4]_2Zn_{1-x}Cu_xCl_4$ were studied as a function of temperature. The chemical shifts in $[N(CH_3)_4]_2Zn_{1-x}Cu_xCl_4$ varied according to the concentration of Cu^{2+} ions. The differences in the chemical shifts among the members of the series could potentially be due to differences in the electron structures of Zn^{2+} and Cu^{2+}, in particular, the structure of the *d* electrons, which screen the nuclear charge from the motion of the outer electrons. Zn^{2+} has a filled *d* shell, whereas Cu^{2+} has one *s* electron outside the closed *d* shell.

$[N(CH_3)_4]_2ZnCl_4$ and $[N(CH_3)_4]_2CuCl_4$ contains two inequivalent types of $N(CH_3)_4$ ions, a-$N(CH_3)_4$ and b-$N(CH_3)_4$, respectively. Here, the two inequivalent kinds of a-$N(CH_3)_4$ and b-$N(CH_3)_4$ in $[N(CH_3)_4]_2Zn_{1-x}Cu_xCl_4$ (x=0, 0.1, 0.3, and 0.5) were not measured. However, the two crystallographically different ions a-$N(CH_3)_4$ and b-$N(CH_3)_4$ in $[N(CH_3)_4]_2CuCl_4$ were identified using ^{13}C CP/MAS NMR. However, the ^1H and ^{13}C $T_{1\rho}$ values were obtained with varying concentrations of Cu^{2+} ions in $[N(CH_3)_4]_2Zn_{1-x}Cu_xCl_4$. It is apparent that $T_{1\rho}$ for ^1H and ^{13}C are not governed by the same mechanism for the amount of paramagnetic impurity Cu^{2+}. As a result, the trends in the NMR spectrum and $T_{1\rho}$ of ^1H and ^{13}C nuclei in the $[N(CH_3)_4]_2Zn_{1-x}Cu_xCl_4$ (x=0.1 and 0.3) were similar to those for $[N(CH_3)_4]_2ZnCl_4$. However, the structural properties of $[N(CH_3)_4]_2Zn_{0.5}Cu_{0.5}Cl_4$ were strongly affected.

The $T_{1\rho}$ values of materials including paramagnetic ions are smaller than those of pure $[N(CH_3)_4]_2ZnCl_4$. Because $T_{1\rho}$ should be inversely proportional to the concentration and to the square of the magnetic moment of the paramagnetic ions, the $T_{1\rho}$ values for samples containing paramagnetic ions are generally smaller than for those without. Therefore, $T_{1\rho}$ for ^1H and ^{13}C are driven in these systems by the fluctuations of the magnetic dipole of the Cu^{2+} paramagnetic ions.

VI. CONCLUSION

The purpose of this study was to investigate how the local structure in a pure crystal is affected by the random presence of a cation of a different size, and to determine the influence of this substitution on the physical properties of the crystal.

After the partial replacement of Zn^{2+} ions by Cu^{2+} ions, the Cu^{2+} ions occupied the same locations in the lattice as the Zn^{2+} ions did. Their crystallographic structures in $[N(CH_3)_4]_2Zn_{1-x}Cu_xCl_4$ (x=0, 0.1, 0.3, 0.5, and 1) can be understood by considering the differences in the chemical shifts of the ^1H MAS NMR and ^{13}C CP/MAS NMR spectra. The NMR spectrum and $T_{1\rho}$ for x=0.1 and 0.3 were similar to those for pure $[N(CH_3)_4]_2ZnCl_4$, whereas the NMR spectrum and $T_{1\rho}$ for x=0.5 were different.

The variation of the structural geometry, as a function of impurity concentration in the mixed system, was interpreted in terms of the differences in size and electron structure between the host and impurity ions. In particular, we attempted to explain the role of CH_3 in the spin-lattice relaxation time mechanisms for the systems containing the paramagnetic Cu^{2+} impurity, based on the ^1H MAS NMR and ^{13}C CP/MAS NMR data in $[N(CH_3)_4]_2ZnCl_4$ and $[N(CH_3)_4]_2CuCl_4$. Consequently, the existence of ferroelastic properties of $N(CH_3)_4$ ions in $[N(CH_3)_4]_2Zn_{1-x}Cu_xCl_4$ (x=0, 0.1, 0.3, and 1) were apparent at low temperatures, whereas they were absent for $[N(CH_3)_4]_2Zn_{0.5}Cu_{0.5}Cl_4$. This study has shown that the replacement of Zn^{2+} ions with a high concentration of Cu^{2+} ions causes the ferroelastic property of the structure to disappear.

ACKNOWLEDGMENT

This research was supported by the Basic Science Research program through the National Research Foundation of Korea (NRF) funded by the Ministry of Education, Science, and Technology (2012001763).

REFERENCES

[1] J. D. Axe, Incommensurate phases in Dielectrics, ed. R. Blinc and A. P. Levanyuk (North-Holland, Amsterdam, 1986).

[2] H. Z. Cummins, Phys. Rep. **185**, 211 (1990).

[3] I. R. Larrea, A. Lopez Echarri, and M. J. Tello, J. Phys. C: Solid State Phys. **14**, 3171 (1981).

[4] M. Hohioka, J. Phys. Soc. Jpn. **52**, 4056 (1983).

[5] S. Sawada, I. Yamaguchi, H. Suzuki, and F. Shimizu, J. Phys. Soc. Jpn. **54**, 3129 (1985).

[6] K. Parlinski and F. Denoyer, J. Phys. C: Solid State Phys. **18**, 293 (1985).

[7] G. Madariaga, F. J. Zuniga, J. M. Perez-Mato, and M. J. Tello, Acta Cryst. B **43**, 356 (1987).

[8] B. Martin, J. M. Pastar, F. Rull, and J. A. De Saja, Solid State Commun. **44**, 1047 (1982).

[9] A. G. Cuevas, M. J. Tello, J. Fernandez, A. L. Echarri, J. herreros, and M. Couzi, J. Phys. C: Solid State Phys. **16**, 473 (1983).

[10] K. Aizu, Phys. Rev. B **2**, 754 (1970).

[11] A. A. El.Fadl, A. El-Korashy, and H. El-Zahed, J. Phys. Chem.Solids **63**, 375 (2002).

[12] A. El-Korashy, J.Materials Science Letters **19**, 29 (2000).

[13] V. B. Kapustyanyk and A. Y. Batyuk, J. Appl. Spectroscopy **71**, 387 (2004).

[14] S. A. Sveleba, I. V. Karpa, I. M. Katerynchuk, O. V. Semotyuk, R. M. Shymkiv, I. M. Kunyo, O. I. Fitsych, J. Appl. Spectroscopy **78**, 228 (2011).

[15] D. G. Sannikov, Phys. Solid State **47**, 324 (2005).

[16] D. G. Sannikov and G. A. Kessenikh, Phys. Solid State **47**, 729 (2005).

[17] D. G. Sannikov, Phys. Solid State **42**, 2282 (2000).

[18] A. Y. Batyuk, V. B. Kapustyanyk, and Y. M. Korchak, J. Appl. Spectro. **72**, 413 (2005).

[19] R. M. Shymkiv, S. A. Sveleba, I. V. Karpa, I. N. Katerynchuk, I. M. Kunyo, and E. I. Phitsych, J. Appl. Spectroscopy **78**, 823 (2011).

[20] A. El. Korashy and M.G. Brik, Solid State Commun. **135**, 298 (2005).

[21] M. Ribet, S. Leon, F. Lefaucheux, and M. C. Robert, J. Appl. Cryst. **23**, 277 (1990).

[22] A. R. Lim and K.-Y. Lim, Solid State Science, **31**, 70 (2014).

[23] A. R. Lim, J. Mol. Structure **1056-1057**, 233 (2014).

[24] A. R. Lim, D. K. Park, J.-H. Chang, and S.-Y. Jeong, J. Phys. Soc. Jpn. **70**, 1937 (2001).

[25] A. B. Rhaiem, F. Hiel, K. Geidara, and M. Gargouri, Spectrochimica Acta A **66**, 1107 (2007).

[26] F. Hlel, A. B. Rhaiem, and K. Guidara, Russ. J. Inorg. Chem. **53**, 785 (2008).

[27] K. Hasebe, H. Mashiyama, N. Koshiji, and S. Tanisaki, J. Phys. Soc. Jpn. **56**, 3543 (1987).

[28] F. J. Zuniga, G. Madariaga, and J. M. Perez-Mato, Acta Cryst. B **45**, 462 (1989).

[29] W. Rehwald and A. Vonlanthen, Z. Phys. B: Condens. Matter **61**, 25 (1985).

[30] K. Gesi and M. Iizumi, J. Phys. Soc. Jpn. **48**, 1775 (1980).

[31] SMART and SAINT-Plus v6.22, Bruker AXS Inc., Madison, Wisconsin, USA, 2000.

[32] J. L. Koenig, Spectroscopy of Polymers (Elsevier, New York 1999).

[33] B. Cowan, Nuclear Magnetic Resonance and Relaxation (Cambridge Univ. UK 1997).

[34] N. Bloembergen, E. M. Purcell, and R. V. Pound, Phys. Rev. **73**, 679 (1948).

FIGURE CAPTIONS

Fig. 1. The structure of $[N(CH_3)_4]_2Zn_{0.5}Cu_{0.5}Cl_4$ in the ab-plane. $Cu/ZnCl_4^{2-}$ anions are represented by grey tetrahedrons. $N(CH_3)_4^+$ cations are represented by empty tetrahedrons. The dashed boundaries show the development of the zigzag chain in the organic-inorganic layer along the [110] direction.

Fig. 2. The colors of mixed crystals $[N(CH_3)_4]_2Zn_{1-x}Cu_xCl_4$ (x=0, 0.1, 0.3, 0.5, and 1).

Fig. 3. Differential scanning calorimetry (DSC) thermogram of $[N(CH_3)_4]_2Zn_{1-x}Cu_xCl_4$ (x=0.1, 0.3, and 0.5) single crystals.

Fig. 4. (a) Chemical shifts of the ^1H MAS NMR spectrum as a function of temperature in $[N(CH_3)_4]_2Zn_{1-x}Cu_xCl_4$ (x=0, 0.1, 0.3, and 0.5) and (b) chemical shift of the ^1H MAS NMR spectrum as a function of temperature in $[N(CH_3)_4]_2CuCl_4$ (x= 1). (Inset: ^1H MAS NMR spectrum for $[N(CH_3)_4]_2CuCl_4$ at room temperature).

Fig. 5. Temperature dependences of the ^1H spin-lattice relaxation time in the rotating frame, $T_{1\rho}$, in $[N(CH_3)_4]_2Zn_{1-x}Cu_xCl_4$ (x=0, 0.3, and 0.5). (Inset: temperature dependences of the ^1H spin-lattice relaxation time in the rotating frame, $T_{1\rho}$, in $[N(CH_3)_4]_2CuCl_4$.

Fig. 6. (a) Chemical shifts of the ^{13}C CP/MAS NMR spectrum as a function of temperature in $[N(CH_3)_4]_2Zn_{1-x}Cu_xCl_4$ (x=0, 0.1, 0.3, and 0.5), (b) In-situ ^{13}C CP/MAS NMR spectrum as a function of temperature in $[N(CH_3)_4]_2Zn_{0.5}Cu_{0.5}Cl_4$, and (c) domain wall patterns of $[N(CH_3)_4]_2Zn_{1-x}Cu_xCl_4$ (x=0, 0.3, and 0.5) at 250 K and 350 K obtained with optical polarizing microscopy.

Fig. 7. (a) Chemical shift of the ^{13}C CP/MAS NMR spectrum as a function of temperature in $[N(CH_3)_4]_2CuCl_4$ (x=1) and (b) domain wall patterns of $[N(CH_3)_4]_2CuCl_4$ at 250 K and 350 K obtained with optical polarizing microscopy.

Fig. 8. (a) Temperature dependences of the ^{13}C spin-lattice relaxation time in the rotating frame, $T_{1\rho}$, in $[N(CH_3)_4]_2Zn_{1-x}Cu_xCl_4$ (x=0, 0.3, and 0.5) and (b) temperature dependences of the ^{13}C $T_{1\rho}$ in $[N(CH_3)_4]_2CuCl_4$.

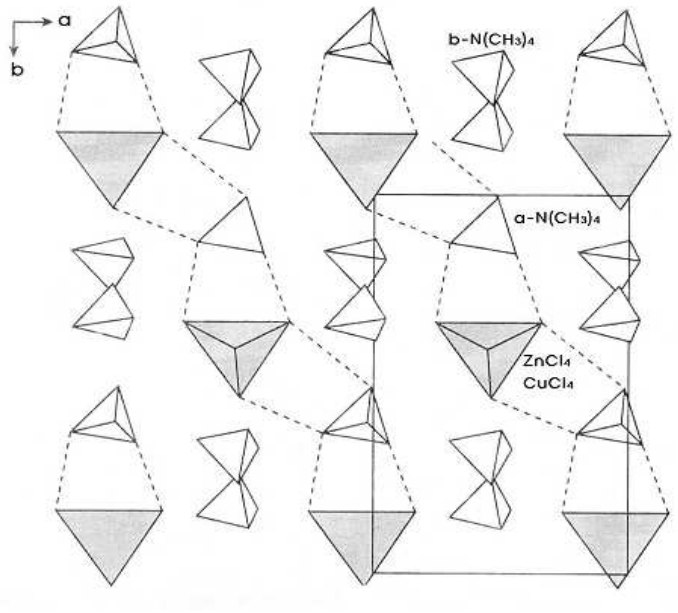

Fig. 1

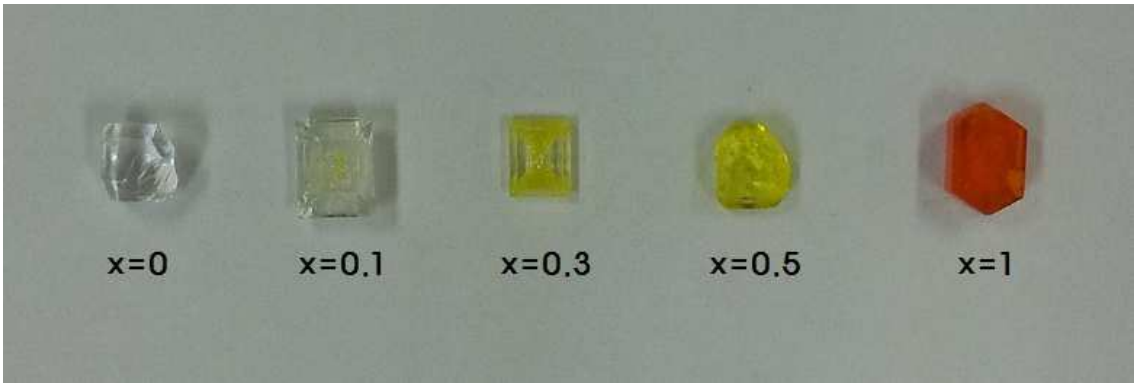

Fig. 2

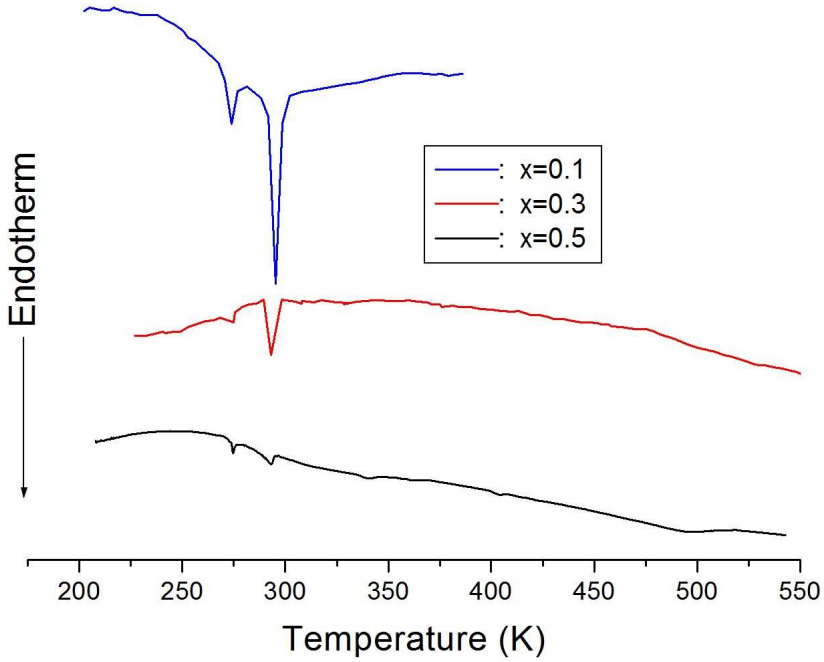

Fig. 3

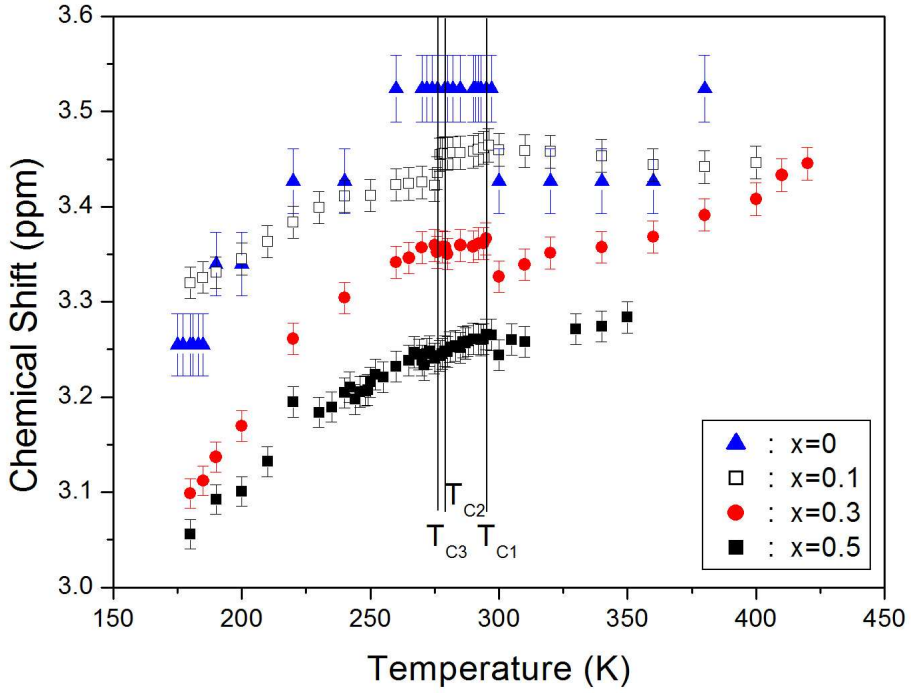

Fig. 4(a)

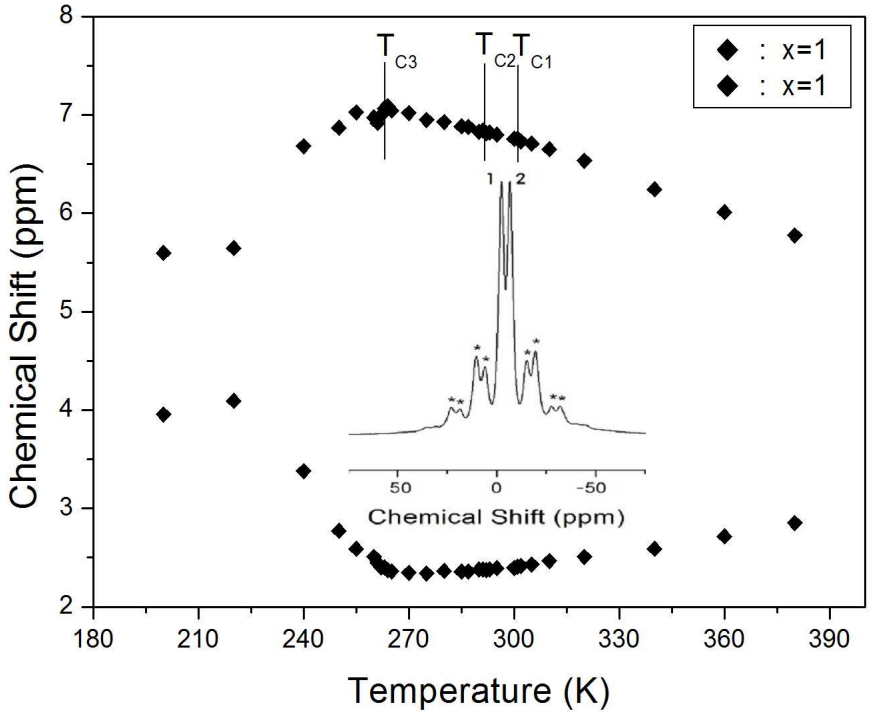

Fig. 4(b)

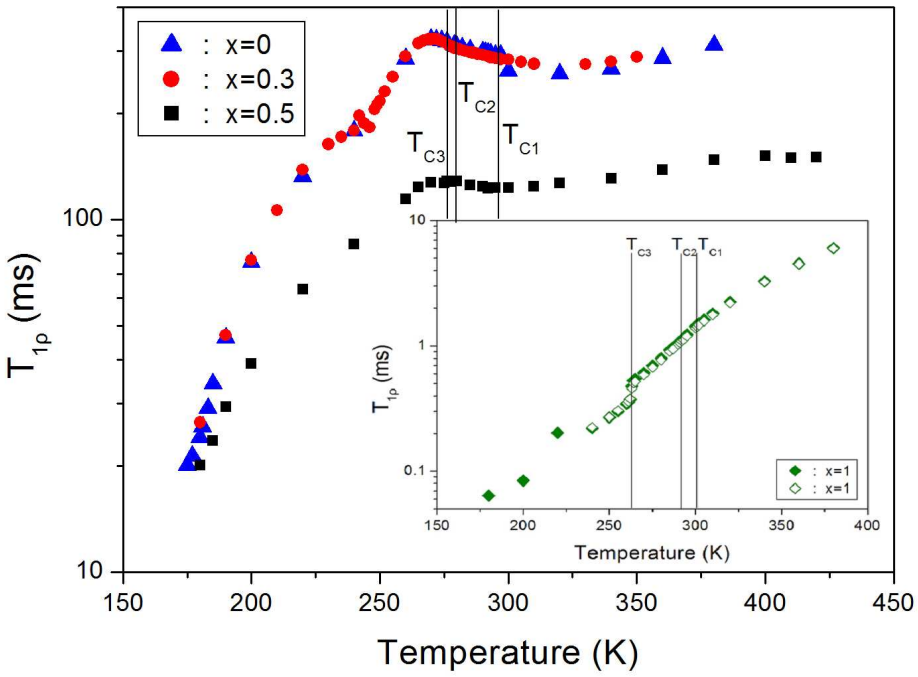

Fig. 5

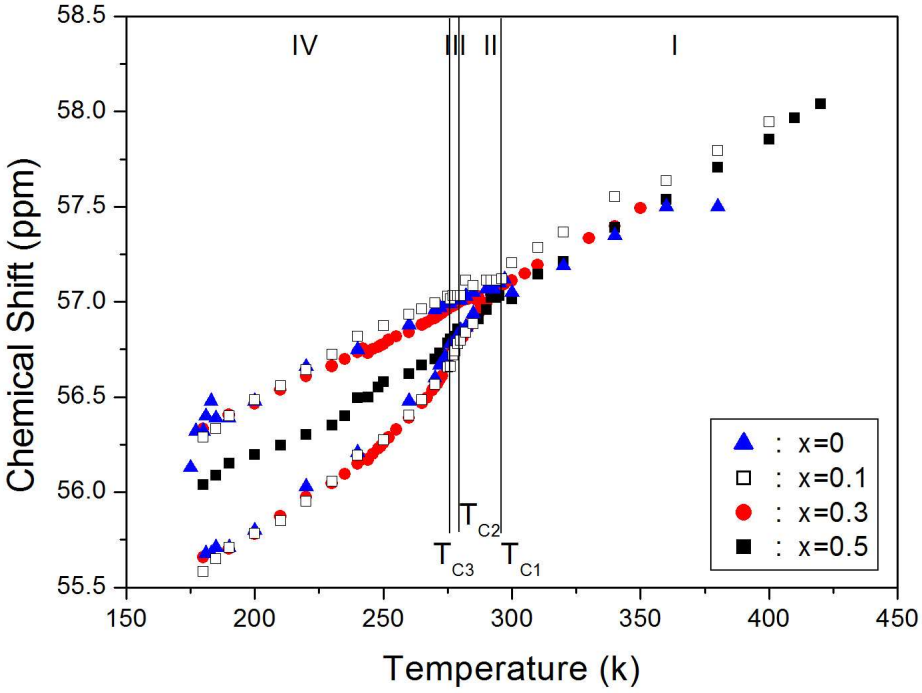

Fig. 6(a)

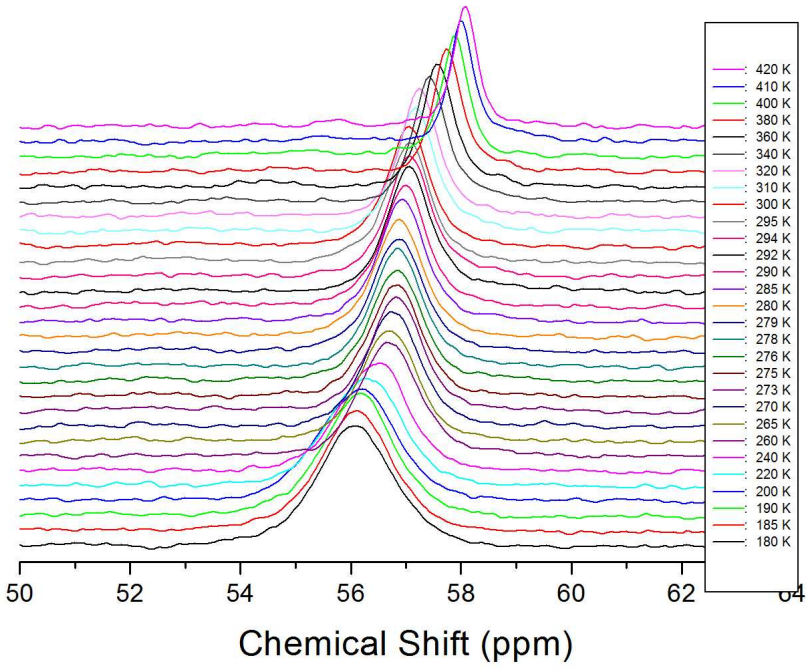

Fig. 6(b)

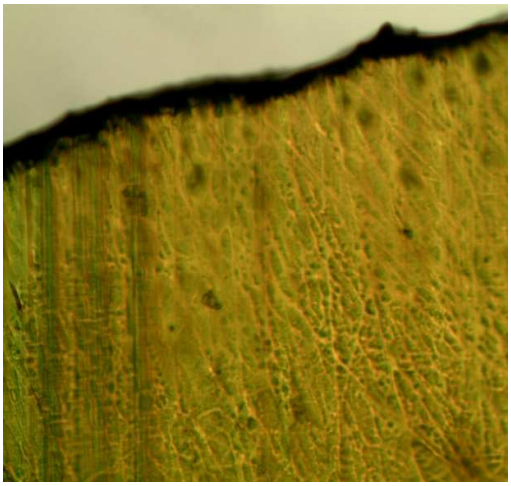

$x = 0$ and $x = 0.3$ at 250 K

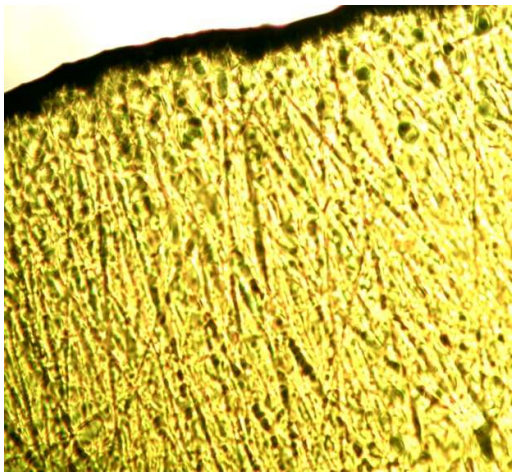

$x = 0$ and $x = 0.3$ at 350 K

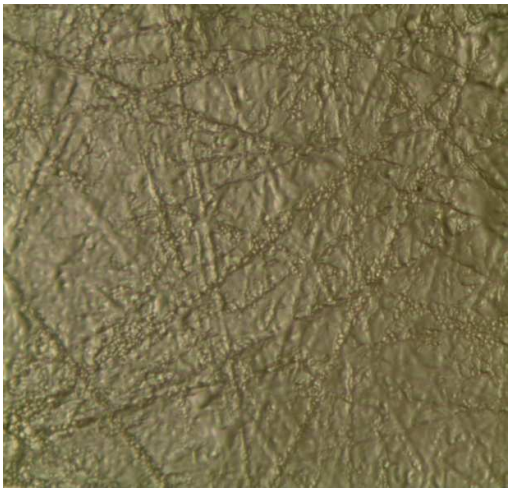

$x = 0.5$ at 250 K

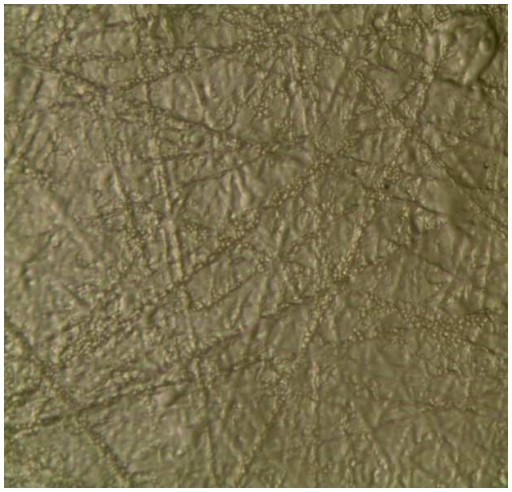

$x = 0.5$ at 350 K

Fig. 6(c)

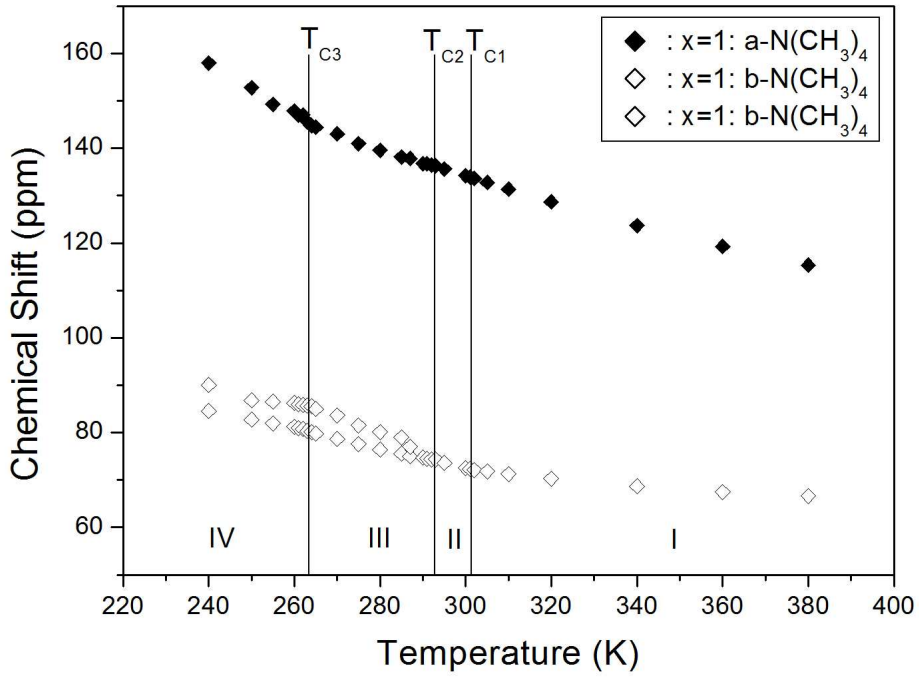

Fig. 7(a)

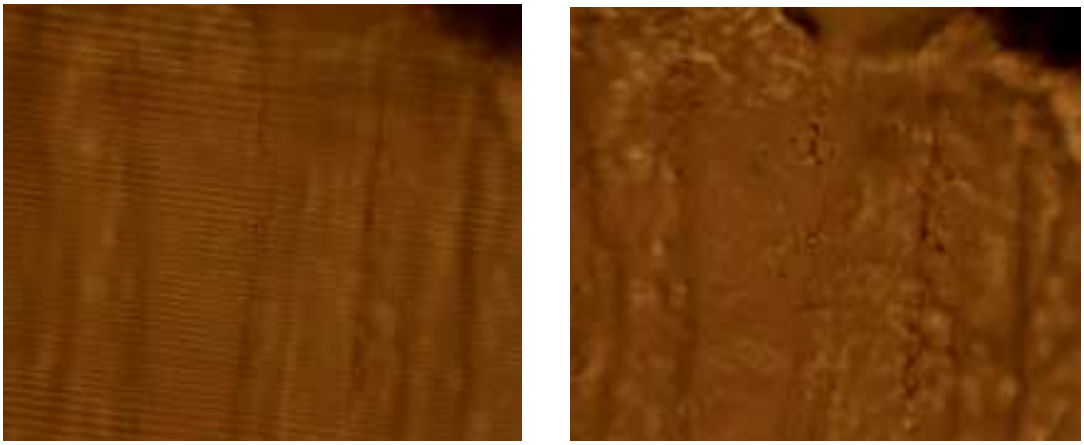

x = 1 at 250 K

x = 1 at 350 K

Fig. 7(b)

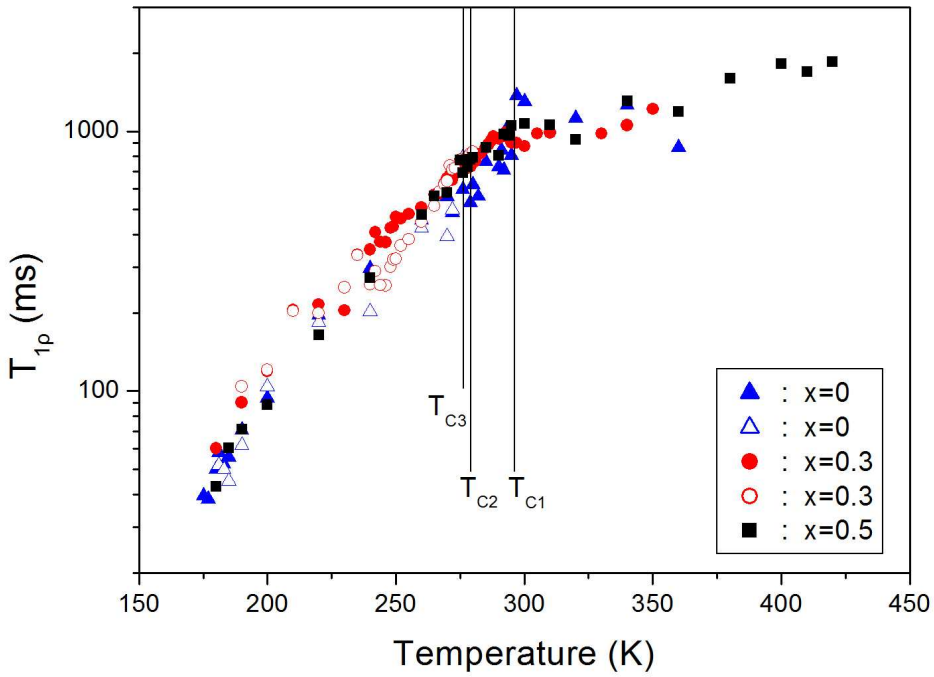

Fig. 8(a)

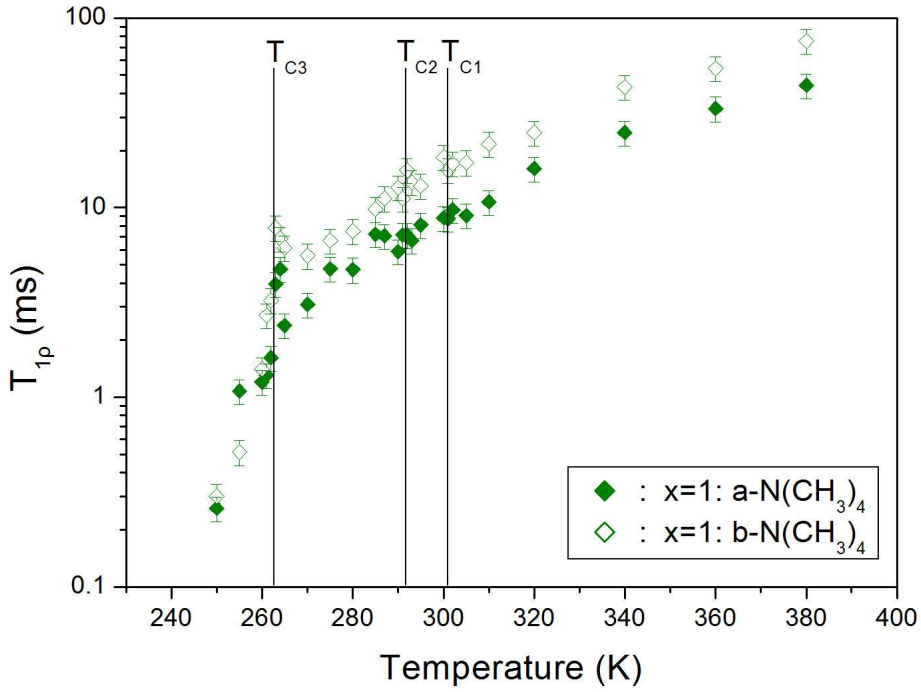

Fig. 8(b)

Table 1. The lattice constants of $[N(CH_3)_4]_2Zn_{1-x}Cu_xCl_4$ (x=0, 0.1, 0.3, 0.5, and 1) at room temperature.

	a	*b*	*c*
$[N(CH_3)_4]_2ZnCl_4$ (x=0)	8.9958 ± 0.0030	15.5162 ± 0.0039	12.2517 ± 0.0034
$[N(CH_3)_4]_2Zn_{0.9}Cu_{0.1}Cl_4$ (x=0.1)	8.9994 ± 0.0027	15.5164 ± 0.0037	12.2713 ± 0.0029
$[N(CH_3)_4]_2Zn_{0.7}Cu_{0.3}Cl_4$ (x=0.3)	8.9988 ± 0.0020	15.5388 ± 0.0035	12.2663 ± 0.0035
$[N(CH_3)_4]_2Zn_{0.5}Cu_{0.5}Cl_4$ (x=0.5)	9.0068 ± 0.0027	15.5409 ± 0.0043	12.2774 ± 0.0032
$[N(CH_3)_4]_2CuCl_4$ (x=1)	9.1136 ± 0.0029	15.2723 ± 0.0046	12.1526 ± 0.0050

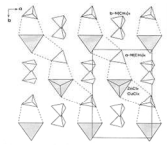

300x208mm (144 x 144 DPI)

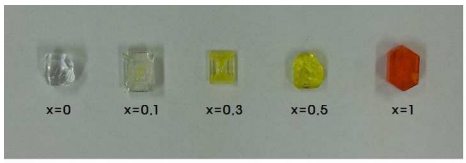

299x209mm (144 x 144 DPI)

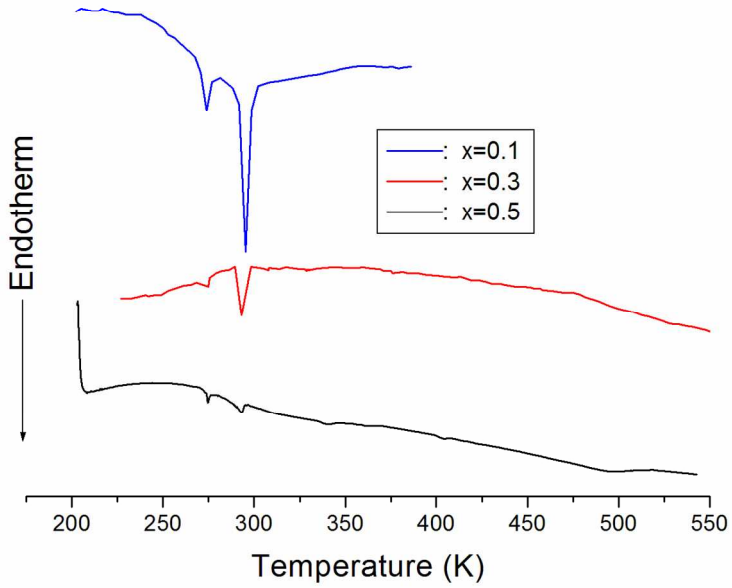

286x201mm (150 x 150 DPI)

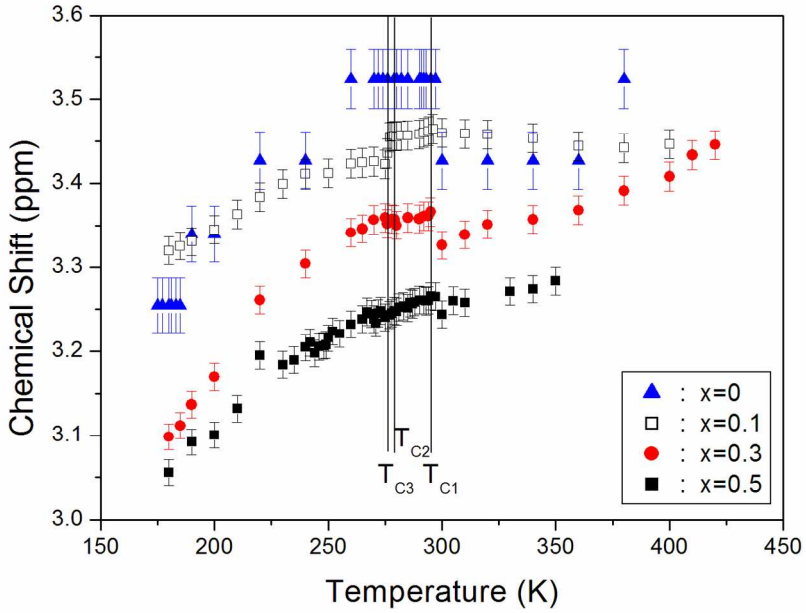

286x201mm (150 x 150 DPI)

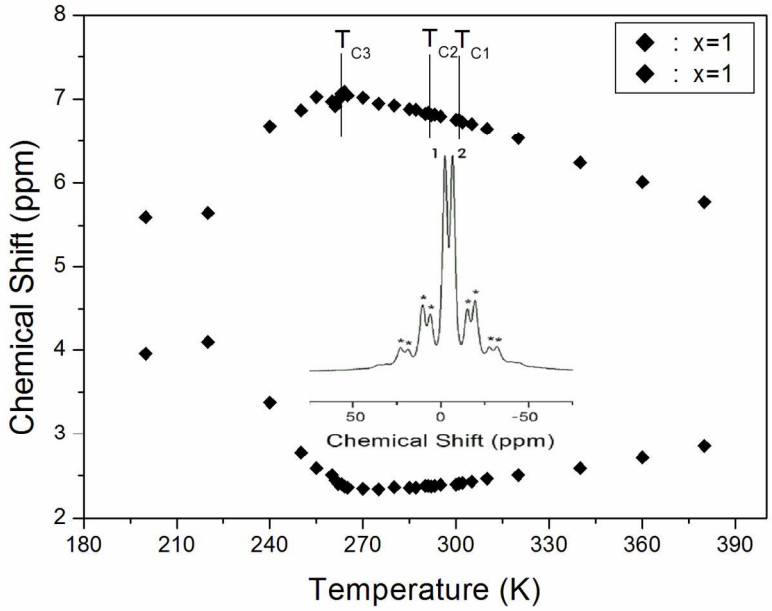

287x201mm (150 x 150 DPI)

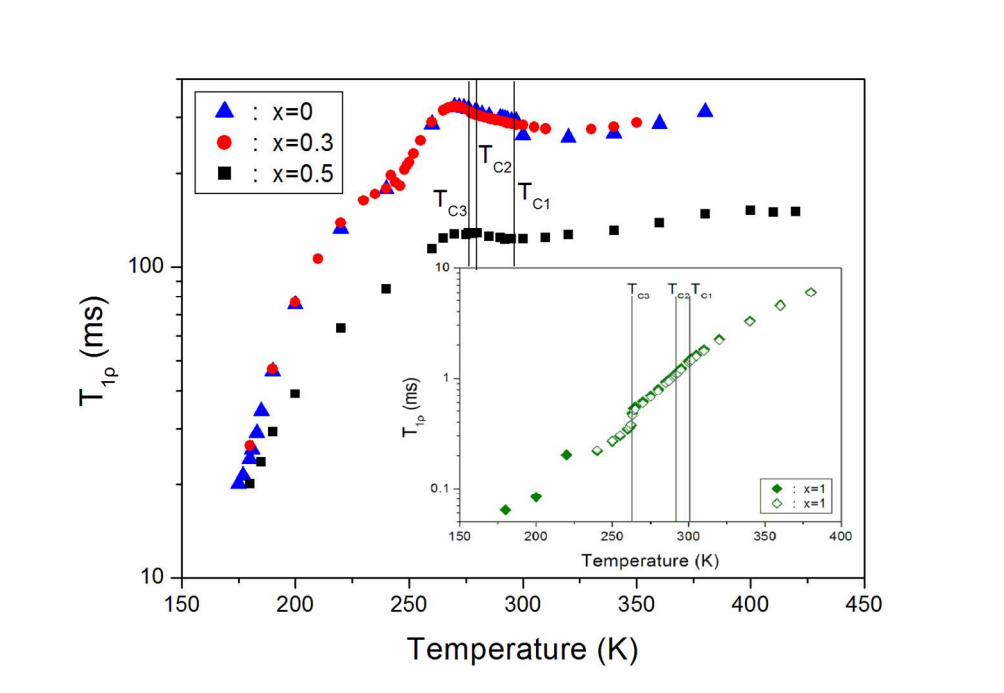

288x200mm (150 x 150 DPI)

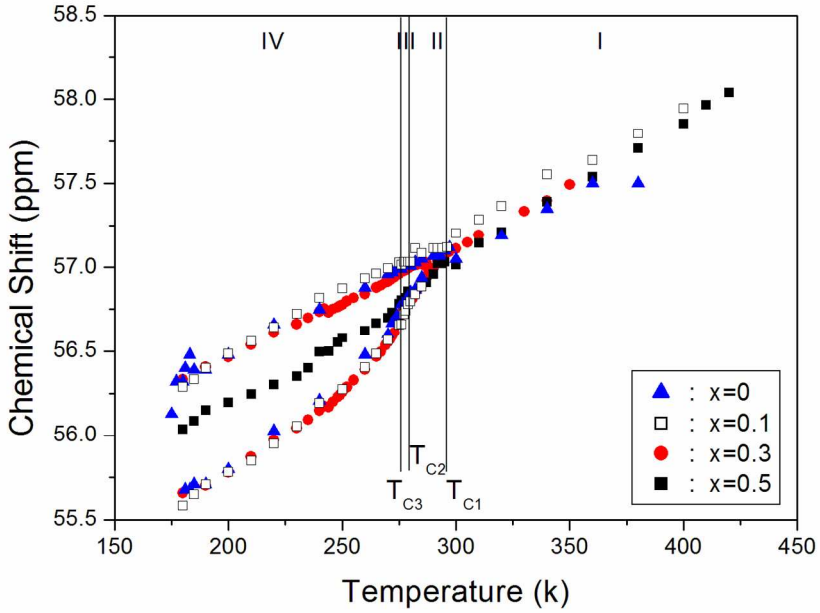

286x201mm (150 x 150 DPI)

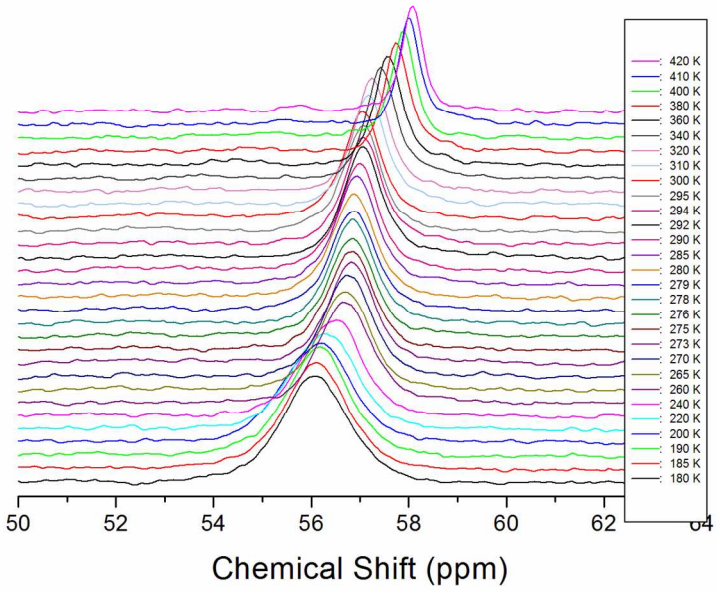

286x201mm (150 x 150 DPI)

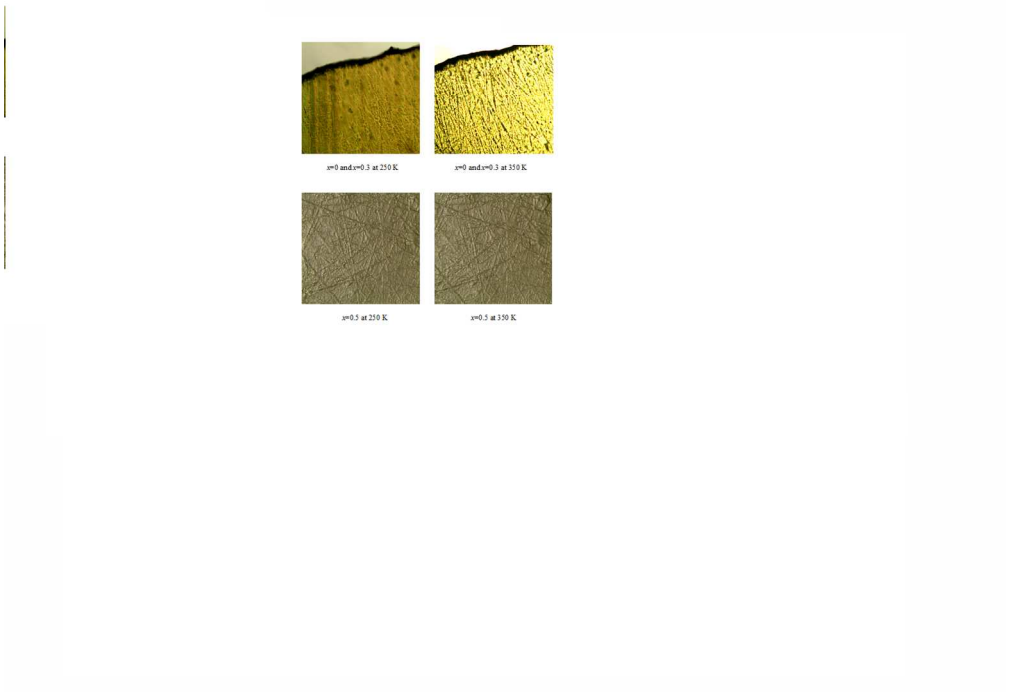

451x313mm (96 x 96 DPI)

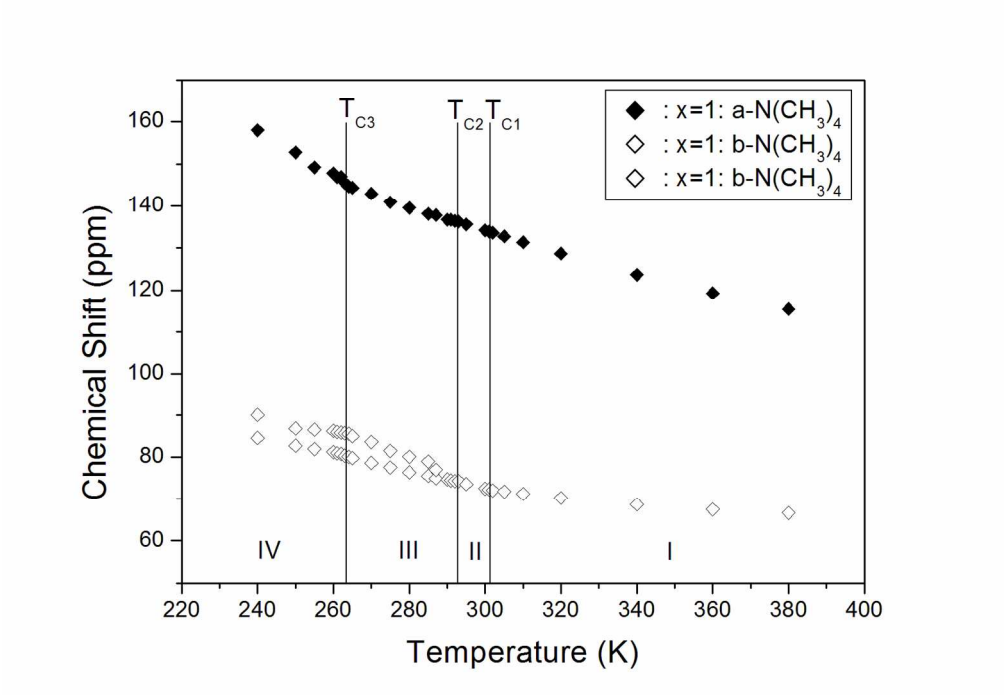

287x201mm (150 x 150 DPI)

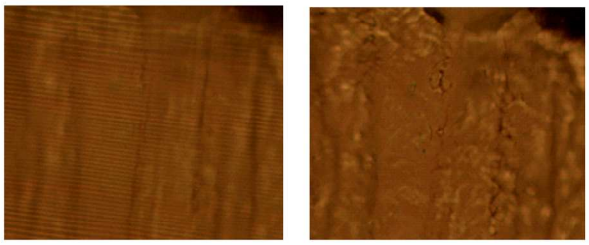

x = 1 at 250 K x = 1 at 350 K

300x208mm (144 x 144 DPI)

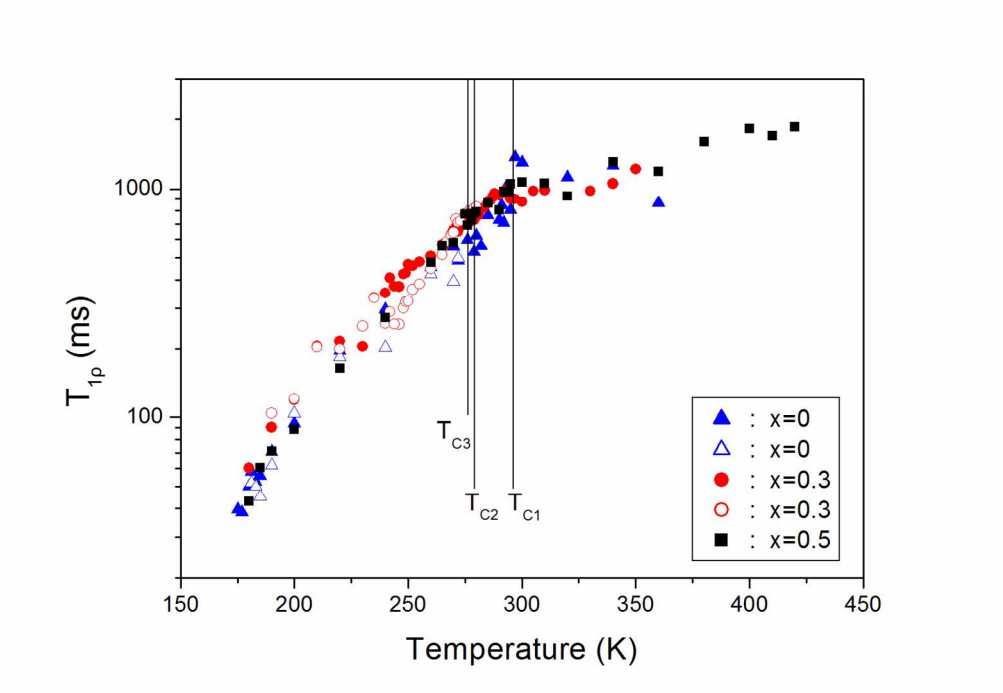

288x200mm (150 x 150 DPI)

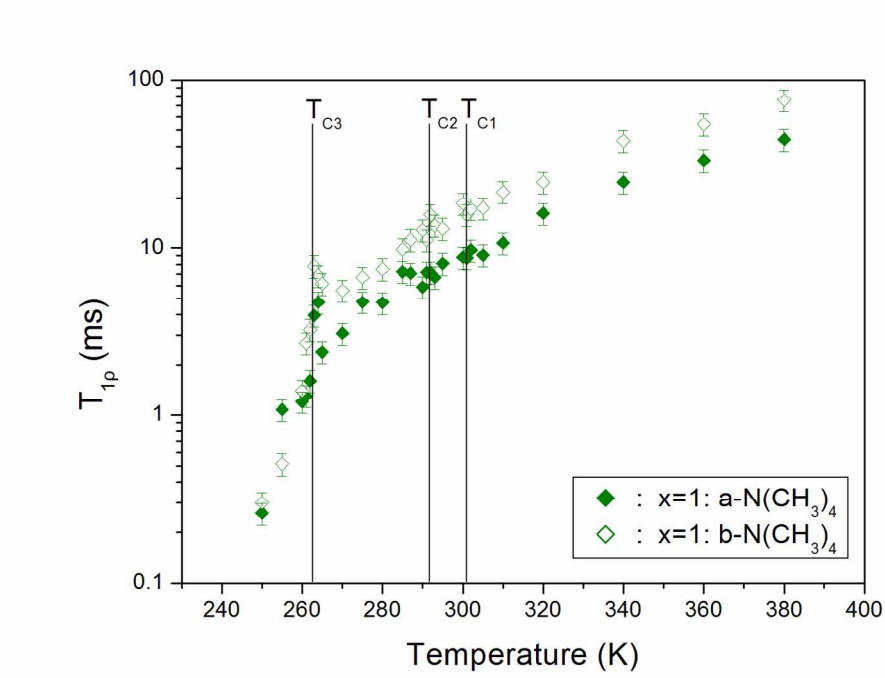

287x201mm (150 x 150 DPI)